Metals and Materials International (2022) 28:1038–1046
https://doi.org/10.1007/s12540-020-00964-7

Effect of Rotary Forging on Microstructure Evolution and Mechanical Properties of Aluminum Alloy/Copper Bimetallic Material

S. O. Rogachev[1] · V. A. Andreev[2,3] · V. S. Yusupov[2] · S. A. Bondareva[1] · V. M. Khatkevich[1,4] · E. V. Nikolaev[1]

Received: 2 December 2020 / Accepted: 28 December 2020 / Published online: 8 May 2021

Abstract
The influence of a degree of strain by rotary forging, as well as post-deformation annealing on the structure and mechanical properties of a clad aluminum alloy/copper bimetallic material was studied. Rotary forging of the initial bimetallic billet was carried out step by step from a diameter of 20.1 mm to a diameter of 2.4 mm. Rotary forging of the aluminum alloy/copper bimetallic material to a diameter of 5.3 mm leads to the formation of a mixed fine-grained and nanocrystalline oriented structure in an aluminum shell and to a decrease in the average grain size by 4.5 times and to an increase in the density of crystalline defects in a copper core. A reduction in the aluminum alloy/copper bimetallic material diameter to 2.4 mm (with intermediate annealing) leads to the formation of a fine-grained elongated grain-subgrain oriented structure in the aluminum shell and to the formation of a mixed cellular and subgrain structure in a copper core. Rotary forging leads to a significant increase in the strength of the aluminum alloy/copper bimetallic material and to a decrease in ductility. The optimal combination of increased strength and satisfactory ductility provides post-deformation annealing.

Keywords Clad Al/Cu bimetallic material · Rotary forging · Nanocrystalline materials · Microstructure · Compounds · Stress/strain measurements

1 Introduction

Hybrid materials are widely used in many industries due to a unique set of properties different from the properties of the hybrid material components separately [1–6]. To date, a wide range of hybrid materials with various architectures from clad to multi-layer and multi-fiber has been developed. One of the popular types of hybrid material is the aluminum-copper system used in electrical engineering and electric power industry [7–10]. However, the low level of strength of such material limits its wider implementation.

The production process, including the selection of hybrid material components and the design of the sequences of their stacking, as well as the applied production technology, significantly affects the final properties of the hybrid material. Therefore, the production of laminated clad material with optimized properties is a problem.

It is known that the formation of ultrafine-grained structures in the components of hybrid metallic materials ensures their higher strength [11–14]. The technological process of creating a hybrid material with simultaneous refinement of its grain structure can be carried out at low temperatures through the use of the severe plastic deformation (SPD) methods [15–17]. Using these technologies, excellent adhesion of dissimilar materials can be achieved.

For example, in work [18], an Al/Cu hybrid material with a spiral architecture of one of the components was obtained. The Al/Cu hybrid material was manufactured by the liquid phase method, i.e. by dipping pure copper spirals into melted pure aluminum, and then the Al/Cu ingot was processed by different SPD methods. It was confirmed that Al/Cu hybrid material with spiral architecture exhibit higher yield strength, increased load-bearing capacity and higher strain hardening during deformation than predicted by the rule of

✉ S. O. Rogachev
csaap@mail.ru

1 National University of Science and Technology MISIS, 119049 Moscow, Russia

2 Baikov Institute of Metallurgy and Materials Science RAS, Moscow 119991, Russia

3 Matek-Sma, Ltd., Moscow 117449, Russia

4 Scientific and Technical Center "TMK", Ltd., Moscow 101000, Russia

mixture. It has been shown that the optimal combination of mechanical strength and electrical conductivity of spiral Al/Cu hybrid material can be achieved by appropriate selection of the SPD mode and subsequent annealing.

To obtain long metal billets, it is promising to use the plastic deformation methods such as rotary forging (swaging) or radial forging [19–22]. These methods can be referred to as the severe plastic deformation methods, since they allow to achieve very high degrees of strain in the billet. Due to rotary forging, it provides more hardening during cold plastic deformation than the rolling method, if we compare the same change in cross section. This is caused by excessive work of deformation of successive impacts of the anvils during rotary forging. The advantage of rotary forging is the possibility of its application in industry. Despite the fact that rotary forging has been known for a long time, little attention is paid to the production of clad materials using this technology. A number of known works on the creation of layered and fibrous Al/Cu materials by rotary forging is small [23, 24]. In these studies, pure aluminum and copper were used as the hybrid material components. At the same time, it is of interest to use a multicomponent aluminum alloy as one of the components of the billet, because the presence of second-phase particles in the aluminum alloy will affect the structure formation during rotary forging and may contribute to the formation of a more dispersed structure [25–27].

The aim of this work is to obtain a clad aluminum alloy/copper bimetallic material by rotary forging and to study the influence of the degree of strain, as well as post-deformation annealing on the change in its structure and mechanical properties.

2 Materials and Methods

The initial bimetallic billet consisted of a copper core with a diameter of 10 mm, placed in an aluminum alloy shell with an external diameter of 20.1 mm. The initial length of the bimetallic billet was 200 mm. The components of the bimetallic billet were obtained by machining the bars from the aluminum alloy grade D16 (2024 type) and copper with a purity of 99.95%, which were subjected to softening annealing before assembly of the bimetallic billet. The chemical composition of the raw materials is presented in Tables 1 and 2.

The aluminum alloy/copper bimetallic material was processed using the modernized double-anvil rotary forging machine RFM1 (B2129.01) (from diameter 20.1 to 5.5 mm), RFM3 (B2127.01) (from diameter 5.5 to 4 mm) and RFM4 (B2123.01) (from diameter 4 to 2.4 mm) without heating, at room temperature. The reduction per pass was 8%–35%. Starting from a diameter of 3.8 mm, a periodic low-temperature annealing of the aluminum alloy/copper bimetallic material to soften a metal was carried out at a temperature of 120 °C in a PTS-2000-60-1200 tube furnace. The final diameter of the aluminum alloy/copper bimetallic material was 2.4 mm. The process of making the aluminum alloy/copper bimetallic material is described in more detail in [28].

Annealing of the aluminum alloy/copper bimetallic material after rotary forging was carried out in a muffle electric furnace in air at temperatures from 180 to 240 °C with a holding time of 30 min to 3 h.

The metallographic analysis of the structure of the aluminum alloy/copper bimetallic material and its components was carried out using an Axio Scope A1 optical microscope (Carl Zeiss) at magnifications up to × 1000 after etching of the cross-section in 50% nitric acid solution (for copper) and 5% HF solution (for aluminum alloy).

The microstructure of the aluminum alloy/copper bimetallic material and its components was studied by transmission electron microscopy (TEM) using a JEM-2100 microscope with EDS. The samples for studying microstructure were prepared in the longitudinal direction using a Strata 201 SIMSmapIII × P scanning ion microscope using a gallium liquid metal ion gun.

The uniaxial tension tests of the aluminum alloy/copper bimetallic material and its components (with a total length of 100 mm and a length of the gage part of 20 mm) were carried out using an universal testing machine INSTRON 150LX at room temperature with a tensile rate of 1 mm/min.

Table 1 The chemical composition of copper (mass%)

Cu	Fe	Ni	Sn	Ag	Pb	Zn	Other impurities
99.97	0.003	0.003	0.002	0.001	0.005	0.003	< 0.01

Table 2 The chemical composition of the aluminum alloy (mass%)

Al	Fe	Si	Mn	Cr	Ti	Cu	Mg	Zn	Other impurities
92.32	0.30	0.26	0.78	0.02	0.05	4.37	1.75	0.14	< 0.01

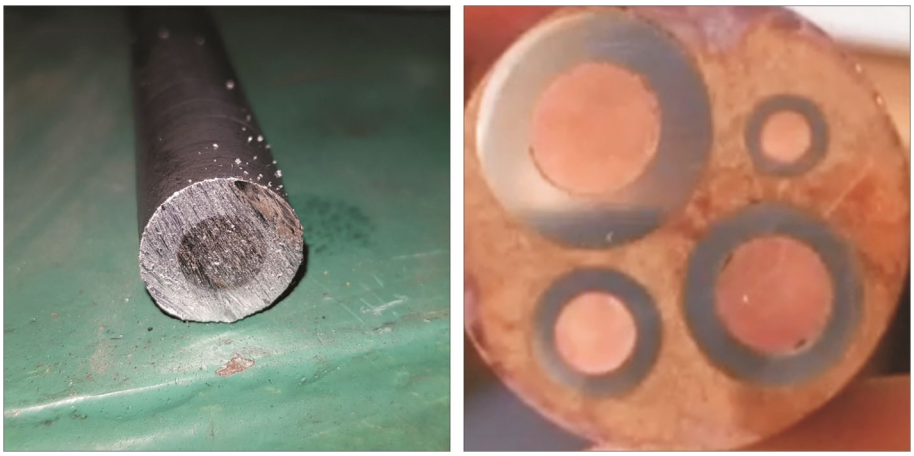

Fig. 1 Appearance of the samples of the aluminum alloy/copper bimetallic material with different diameters after rotary forging

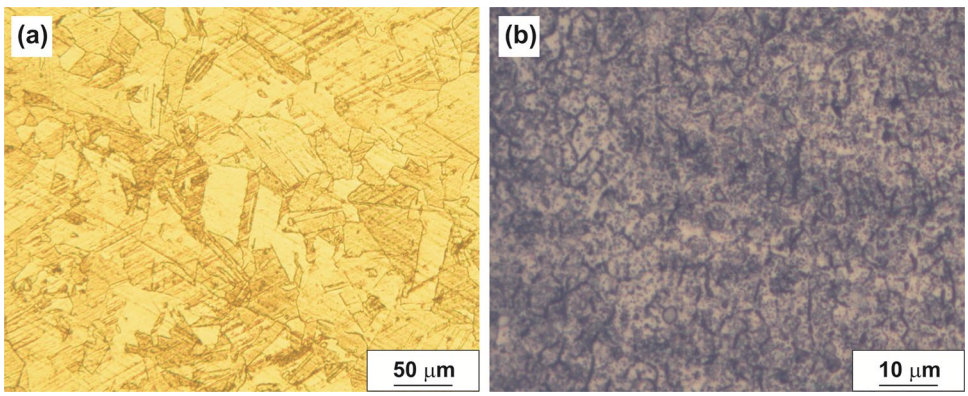

Fig. 2 The microstructure of copper (**a**) and aluminum alloy (**b**) in the annealed state (optical microscopy)

3 Results and Discussion

3.1 The Effect of Rotary Forging on the Structure of the Aluminum Alloy/Copper Bimetallic Material

The rotary forging method was used to obtain long-length clad aluminum alloy/copper bimetallic material. The length of the aluminum alloy/copper bimetallic material with a final diameter of 2.4 mm was over 10 m. Due to the different deformability of copper and aluminum alloy, a different change in the outer diameter of the aluminum alloy/copper bimetallic material and the diameter of the copper rod was observed during the forging process. When the outer diameter of the aluminum alloy/copper bimetallic material decreases from 20.1 ± 0.1 to 5.3 ± 0.1 and to 2.4 ± 0.1 mm, the diameter of the copper core decreases from 9.8 ± 0.1 to 2.9 ± 0.1 and to 1.4 ± 0.1 mm. The appearance of the samples of the aluminum alloy/copper bimetallic material after rotary forging is shown in Fig. 1.

Table 3 Results of chemical analysis of inclusions in the structure of the aluminum alloy in the annealed state (according to TEM with EDS)

Spectrum number	Element	Mass%	at%	Compound
1	Al	61.5	77.4	$(CuFeMn)_3Si_2Al_{15}$
	Mn	19.4	12.0	
	Cu	17.6	9.4	
	Fe	1.0	0.6	
	Si	0.4	0.5	
2	Al	84.2	92.2	$Al_{20}Cu_2Mn_3$
	Cu	8.7	4.1	
	Mn	7.0	3.8	
3	Mg	3.6	4.7	Al_2CuMg
	Al	68.6	81.3	
	Cu	27.8	14.0	

According to optical microscopy, the grain sizes in copper and aluminum alloy of the initial state (after annealing)

were 36 and 3 μm, respectively (Fig. 2).

According to transmission electron microscopy with EDS, the oriented Al_2CuMg, $Al_{20}Cu_2Mn_3$ and $(CuFeMn)_3Si_2Al_{15}$ type particles with a predominant size of 100–500 nm were detected in the structure of aluminum alloy in the annealed state (see Fig. 3 and Table 3). It was shown earlier that the 2024 alloy in the annealed state also contains large Al_2CuMg particles and a small amount of large $(CuFeMn)_3Si_2Al_{15}$ particles (~ 1–5 μm in size) [25]. Obviously, such particles are not detected by TEM due to the small size of the analyzed area (~ 5 × 15 μm), but they are well detected by SEM [28].

Rotary forging of the aluminum alloy/copper bimetallic material leads to a decrease in grain size in the aluminum shell and copper core. When reducing the diameter of the aluminum alloy/copper bimetallic material from 20.1 to 5.3 and to 2.4 mm, the average grain size in the copper core decreases sequentially from 36 to 30 and to 4 μm, respectively (Fig. 4). At the same time, the grain structure in the aluminum shell after rotary forging to a diameter of 5.3 and 2.4 mm does not visible by optical microscopy.

According to transmission electron microscopy with EDS, rotary forging of the aluminum alloy/copper bimetallic material to a diameter of 5.3 mm leads to the formation of a mixed fine-grained and nanocrystalline oriented structure in the aluminum shell (Fig. 5a). The structure shows elongated grains with a cross-section from 100 to 400 nm, consisting of nanocrystalline grains 10–20 nm in size, which are clearly visible in a dark field (Fig. 5b), as well as in bright field at high magnifications (shown by arrows in Fig. 5c, d). The body of most nanoscale grains is light and free from defects. At the same time, the boundaries between nanocrystallites are poorly visible. The presence of precisely a nanocrystalline structure with predominantly high-angle misorientation of the boundaries is indicated by the contrast in the dark-field image, as well as by ring electron diffraction patterns formed by actually contacting point reflexes.

The Al_2Cu and $(CuFeMn)_3Si_2Al_{15}$ type particles with a predominant size of 100–500 nm were detected in the structure (chemical composition is given in Table 4).

A decrease in the diameter of the aluminum alloy/copper bimetallic material to 2.4 mm (with intermediate annealing at 120 °C) leads to the formation of a fine-grained elongated grain-subgrain oriented structure in the aluminum shell (Fig. 6). The structure is less dispersed compared with the structure of the aluminum shell of the aluminum alloy/copper bimetallic material with a diameter of 5.3 mm, as indicated by an intermittent ring electron diffraction pattern. In this case, the density of the crystal lattice defects is higher. The average cross-section size of elongated grains (subgrains) was 0.3 μm.

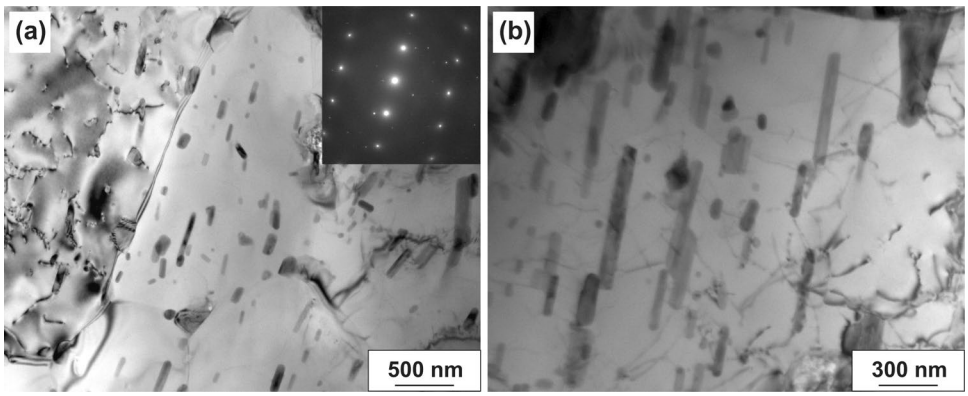

Fig. 3 The microstructure of the aluminum alloy in the annealed state (TEM)

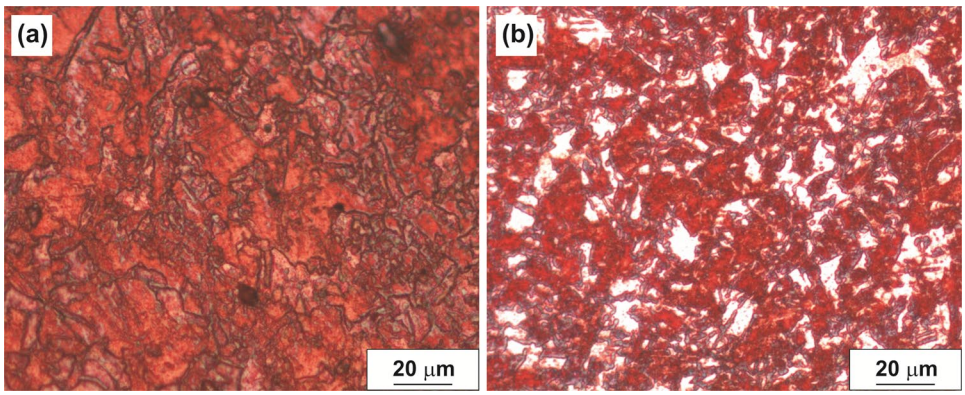

Fig. 4 Microstructure of the copper core of the aluminum alloy/copper bimetallic material after rotary forging to a diameter of (**a**) 5.3 and **b** 2.4 mm (optical microscopy)

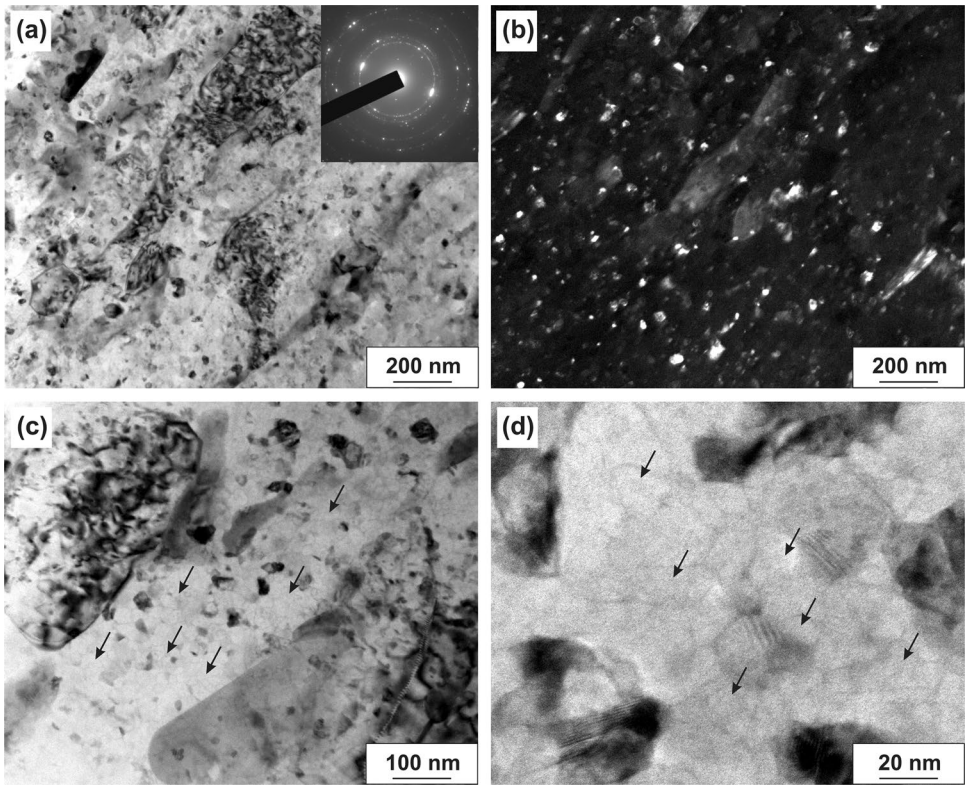

Fig. 5 The microstructure of the aluminum shell of the aluminum alloy/copper bimetallic material after rotary forging to a diameter of 5.3 mm (TEM): **a**, **c**, **d**-bright fields; **b**-dark field in reflexes (Al)

Table 4 Results of chemical analysis of inclusions in the structure of the aluminum alloy shell of the aluminum alloy/copper bimetallic material after rotary forging to a diameter of 5.3 mm (according to TEM with EDS)

Spectrum number	Element	Mass%	at%	Compound
1	Al	60.2	76.8	$(CuFeMn)_3Si_2Al_{15}$
	Mn	12.1	7.6	
	Cu	26.2	14.2	
	Fe	0.7	0.5	
	Si	0.7	0.9	
2	Al	77.9	89.3	Al_2Cu
	Cu	22.1	10.7	

In the structure of the aluminum alloy after forging to a diameter of 2.4 mm, dispersed particles of the Al_2CuMg, Al_2Cu, $Al_{20}Cu_2Mn_3$ and $(CuFeMn)_3Si_2Al_{15}$ types of round and elongated shape with a predominant size of 40–300 nm were also identified (shown by arrows in Fig. 6c); the chemical composition is given in Table 5.

A mixed cellular and subgrain structure was formed in the copper core (Fig. 7). The average cell size formed by the walls of the dislocations was 0.54 μm, and the cross-section size of the subgrains was 0.23 μm.

Thus, TEM studies have shown that rotary forging leads to greater refinement of the grain structure in the aluminum shell, rather than in the copper rod. The most dispersed structure in the aluminum shell is observed for the aluminum alloy/copper bimetallic material diameter of 5.3 mm. In fact, the structure is nanocrystalline. The presence of such a highly dispersed structure in the aluminum shell, in our opinion, may be a consequence of a very large local shear strain achieved in the surface layers of the aluminum alloy/copper bimetallic material during rotary forging.

A change in the structure type of the aluminum shell from a more dispersed to less dispersed one with an increase in reduction of the aluminum alloy/copper bimetallic material (i.e., with an increase in the degree of strain) can be a result of both annealing between passes and the cyclic process of structure formation, which can often be observed during severe plastic deformations [29, 30].

The small $(CuFeMn)_3Si_2Al_{15}$ particles revealed in the structure of the aluminum shell are obviously the large $(CuFeMn)_3Si_2Al_{15}$ particles that were present in the structure of the annealed aluminum alloy and fragmented during forging. At the same time, the Al_2CuMg particles present in the annealed alloy were not detected in the structure of the aluminum shell after rotary forging to a diameter of 5.3 mm. This is probably due to the fact that these particles do not appear in the field of view of the electron microscope due to the small size of the analyzed area, or because of their loss during the sample preparation. An increase in the reduction

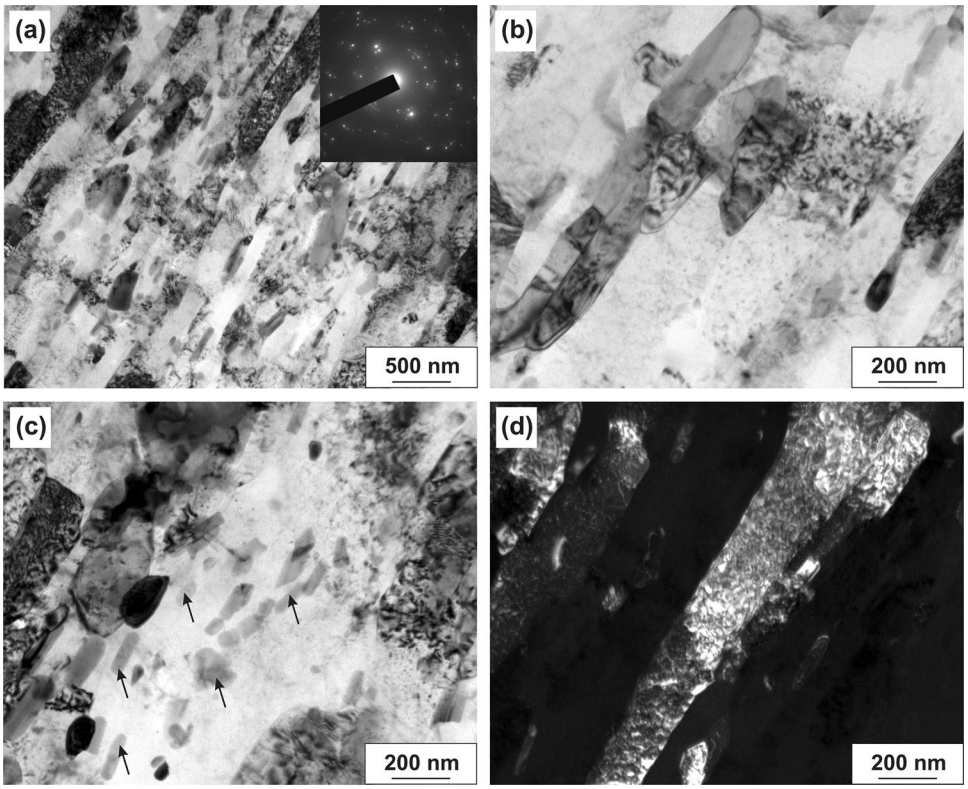

Fig. 6 Microstructure of the aluminum shell of the aluminum alloy/copper bimetallic material after rotary forging to a diameter of 2.4 mm (TEM): **a**, **b**, **c**-bright fields; **d**-dark field in reflections (Al)

Table 5 Results of chemical analysis of inclusions in the structure of the aluminum alloy of the aluminum alloy/copper bimetallic material shell after rotary forging to a diameter of 2.4 mm (according to TEM with EDS)

Spectrum number	Element	Mass%	at%	Compound
1	Al	78.0	88.7	$Al_{20}Cu_2Mn_3$
	Mn	8.5	4.8	
	Cu	13.4	6.5	
2	Al	80.6	90.7	Al_2Cu
	Cu	19.4	9.3	
3	Mg	5.8	9.5	Al_2CuMg
	Al	37.2	54.8	
	Cu	57.0	35.7	
4	Al	63.8	79.4	$(CuFeMn)_3Si_2Al_{15}$
	Mn	16.0	9.8	
	Fe	1.8	1.0	
	Cu	18.5	9.8	

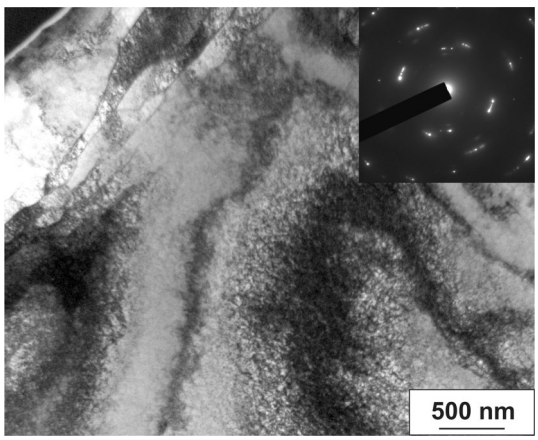

Fig. 7 Microstructure of the copper core of the aluminum alloy/copper bimetallic material after rotary forging to a diameter of 2.4 mm (TEM)

of the aluminum alloy/copper bimetallic material from 5.3 to 2.4 mm leads to refinement of the Al_2CuMg particles.

Considering that no Al_2Cu particles were found in the structure of the aluminum alloy in the initial state, their presence in the structure of the aluminum alloy after forging to diameters of 5.3 and 2.4 mm can be a result of the forging process. The precipitation of excess phases during severe plastic deformations was noted in a number of works [27, 31–33].

It is more difficult to explain the fact that the $Al_{20}Cu_2Mn_3$ particles are detected in the structure of an aluminum alloy of the initial state, than they are not detected after forging to a diameter of 5.3 mm, and they are again revealed after forging to a diameter of 2.4 mm. This circumstance requires additional research, incl. with an increase in statistics. However, it can be noted that in [34] it was shown that in the

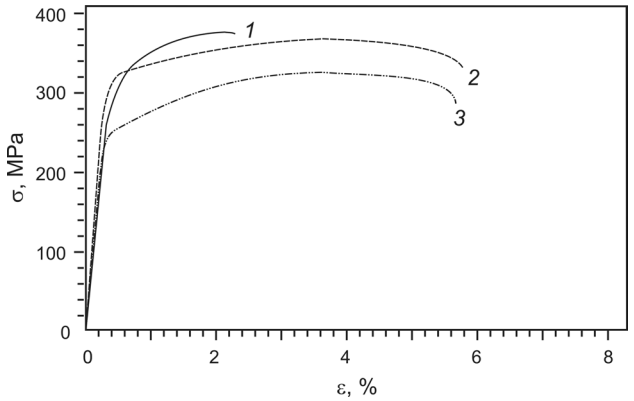

Fig. 8 Tensile test stress–strain curves for the aluminum alloy/copper bimetallic material with a diameter of 5.3 mm after rotary forging (1) and subsequent annealing at 180 °C, 3 h (2) and 240 °C, 1 h (3)

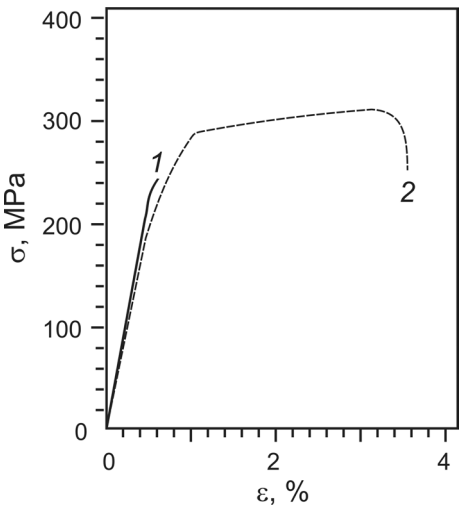

Fig. 9 Tensile test stress–strain curves for the aluminum alloy/copper bimetallic material with a diameter of 2.4 mm after rotary forging (1) and subsequent annealing at 240 °C, 2 h (2)

course of processing multiphase materials (in particular, Cu-Ag alloys) by the SPD-methods, there is a redistribution of alloy components between the matrix of the solid solution and precipitates, and there are two simultaneous processes: dissolution of precipitates and decomposition of a supersaturated solid solution with the precipitation of a second phase.

3.2 The Effect of Rotary Forging on Mechanical Properties of the Aluminum Alloy/Copper Bimetallic Material

The stress–strain curves of the aluminum alloy/copper bimetallic material are shown in Figs. 8 and 9, and the values of the mechanical properties are shown in Table 6.

Rotary forging leads to a significant increase in the strength of the aluminum alloy/copper bimetallic material and to a decrease in ductility. The yield strength and tensile strength of the samples of the aluminum alloy/copper bimetallic material with a diameter of 5.3 mm were, respectively, 330 and 375 MPa, which is 1.6–3.0 times higher than those for the annealed components of the aluminum alloy/copper bimetallic material. However, the elongation of the samples of the aluminum alloy/copper bimetallic material does not exceed 2%. It can be noted that the strength level of the aluminum alloy/copper bimetallic material after rotary forging to a diameter of 5.3 mm is close to the strength level of the Al-Cu-Mg alloy in the quenched state (ultimate strength 370 MPa) and is inferior to the strength level of the same alloy after ECAP [35]. It should be taken into account that with an outer diameter of the aluminum alloy/copper bimetallic material of 5.3 mm, the area of the aluminum shell is 70% of the entire area of the aluminum alloy/copper bimetallic material [28], and the strength of copper, even with a developed cellular substructure, does not exceed 370 MPa, then the strength level of the aluminum shell should exceed 370 MPa.

A reduction in the diameter of the aluminum alloy/copper bimetallic material to 2.4 mm leads to a further decrease in

Table 6 Mechanical properties of the aluminum alloy/copper bimetallic material and its components in various states

Material	Forging to diameter, mm	Annealing (time, temperature)	Yield strength, MPa	Tensile strength, MPa	Elongation, %
Copper bar	–	500 °C, 40 min	122 ± 5	238 ± 4	28 ± 2
Aluminum alloy bar	–	400 °C, 2 h	108 ± 4	220 ± 5	10 ± 1
Bimetallic material	5.3	–	330 ± 6	375 ± 5	2.0 ± 0.3
Bimetallic material	5.3	180 °C, 1 h	355 ± 6	370 ± 5	4 ± 1
Bimetallic material	5.3	180 °C, 3 h	325 ± 5	370 ± 6	6 ± 1
Bimetallic material	5.3	240 °C, 1 h	255 ± 4	325 ± 5	6 ± 1
Bimetallic material	2.4	–	–	230 ± 20	0
Bimetallic material	2.4	180 °C, 3 h	–	260 ± 40	0
Bimetallic material	2.4	240 °C, 2 h	295 ± 5	310 ± 5	3.0 ± 0.5

ductility and premature failure of the sample (at stresses of 210–250 MPa) due to the nucleation (or propagation) of cracks in the aluminum shell at the stage of elastic deformation.

Thus, an increase in strength and a decrease in the ductility of the aluminum alloy/copper bimetallic material after rotary forging is caused by grain structure refinement and increase in crystalline defect density. The embrittlement of the aluminum shell with an increase in the degree of strain of the aluminum alloy/copper bimetallic material is apparently a consequence of an additional increase in the density of crystalline defects and the precipitation of the dispersed particles. It should be noted once again that the material during processing by SPD can pass into a nonequilibrium state, and a certain fraction of chemical elements can segregate along grain boundaries [36]. In the case of multicomponent hybrid materials, segregation can also be expected at the interfaces between the components of the hybrid material. Such segregations can also affect the mechanical properties of the hybrid material.

3.3 The Effect of Annealing After Rotary Forging on Mechanical Properties of the Aluminum Alloy/Copper Bimetallic Material

Annealing of the samples of the aluminum alloy/copper bimetallic material with a diameter of 5.3 mm at a temperature of 180 °C (1 h) after rotary forging does not led to a decrease in their strength, but it increases their ductility (relative elongation increases to 3%–4%) (Fig. 8, Table 6). An increase in the holding time during annealing from 1 to 3 h increases the elongation to 6%. An increase in the annealing temperature to 240 °C (2 h) leads to a decrease in the yield strength and tensile strength of the samples of the aluminum alloy/copper bimetallic material to 255 and 325 MPs, respectively, while maintaining a relative elongation of 6%.

Annealing of the samples of the aluminum alloy/copper bimetallic material with a diameter of 2.4 mm at a temperature of 180 °C (1–3 h) after rotary forging does not led to a change in their mechanical properties (compared with the state after forging) (Fig. 9, Table 6). With increasing annealing temperature to 240 °C (2 h), the yield strength and tensile strength of the samples of the aluminum alloy/copper bimetallic material were 295 and 310 MPa, respectively, with a relative elongation of 3%. The obtained values of yield strength and tensile strength are 1.3–2.7 times higher than those for the initial components.

It should be noted that during the tensile test the copper rod was deformed plastically with the formation of a neck and a significant reduction in diameter after all modes of deformation-heat treatment. At the same time, the deformation of the aluminum shell with a diameter of 5.3 mm develops with the formation of a neck and a very small reduction in diameter, which increased with an increase in the annealing temperature. Deformation of the aluminum shell with a diameter of 2.4 mm proceeded without necking under all modes of deformation-heat treatment.

Thus, the optimal combination of increased strength and satisfactory ductility attractive for use in the electrical industry provides post-deformation annealing of the aluminum alloy/copper bimetallic material.

4 Conclusions

(1) Rotary forging of a clad aluminum alloy/copper bimetallic material from a diameter of 20.1 mm to a diameter of 5.3 mm leads to the formation of a mixed fine-grained and nanocrystalline oriented structure in an aluminum shell and a decrease in the average grain size by 4.5 times and an increase in the density of crystalline defects in a copper core. A reduction in the diameter of the aluminum alloy/copper bimetallic material to 2.4 mm (with intermediate annealing) leads to the formation of a fine-grained elongated grain-subgrain oriented structure in the aluminum shell with precipitation of dispersed particles and the formation of a mixed cellular and subgrain structure in the copper core.

(2) Rotary forging leads to a significant increase in the strength of the aluminum alloy/copper bimetallic material and a decrease in ductility. The optimal combination of increased strength and satisfactory ductility provides post-deformation annealing. The yield strength and tensile strength of the samples of the aluminum alloy/copper bimetallic material with a diameter of 5.3 mm after annealing at 180 °C (3 h) were 325 and 370 MPa (which is 1.5–3.0 times higher than those for the initial components of the aluminum alloy/copper bimetallic material), respectively, with a relative elongation of 6%. The yield strength and tensile strength of the samples of the aluminum alloy/copper bimetallic material with a diameter of 2.4 mm after annealing at a temperature of 240 °C (2 h) were 295 and 310 MPa (which is 1.3–2.7 times higher than those for the initial components of the aluminum alloy/copper bimetallic material), respectively, with a relative elongation of 3%.

Acknowledgements The aluminum alloy/copper bimetallic material forging process was carried out as part of the state assignment IMET RAS No. 075-00947-20-00. Investigation of the aluminum alloy/copper bimetallic material was carried out with partial financial support from the Ministry of Science and Higher Education of the Russian Federation in the framework of Increase Competitiveness Program of NUST MISIS (No. K2-2019-008), implemented by a governmental decree

dated 16th of March 2013, N 211. The authors thank A.A. Tokar for help in preparing samples.

Availability of data and material None.

Compliance with ethical standards

Conflict of interest The authors declare that they have no known competing financial interests or personal relationships that could have appeared to influence the work reported in this paper.

Code availability Not applicable.

References

1. M.F. Ashby, Y.J.M. Brechet, Acta Mater. **51**, 5801 (2003)
2. H.H. Kim, M.S. Lee, C.G. Kang, Mater. Manuf. Process. **28**, 892 (2013)
3. O. Bouaziz, Scripta Mater. **68**, 28 (2013)
4. A. Molotnikov, R. Gerbrand, O. Bouaziz, Y. Estrin, Adv. Eng. Mater. **15**, 728 (2013)
5. A.Y. Nalivaiko, A.N. Arnautova, S.V. Zmanovsky, D.Y. Ozherelkov, P.K. Shurkin, A.A. Gromov, J. Alloy. Compd. **825**, 154024 (2020)
6. S. Mondal, Aluminum or Its Alloy Matrix Hybrid Nanocomposites. Met. Mater. Int. (2020). https://doi.org/10.1007/s12540-020-00750-5
7. I.-K. Kim, S.I. Hong, Mater. Design **47**, 590 (2013)
8. M. Zebardast, A.K. Taheri, J. Mater. Process. Tech. **211**, 1034 (2011)
9. N. Ahmed, J. Mech. Work. Technol. **2**, 19 (1978)
10. Y. Mitani, H. Balmori, in *Strength of Metals and Alloys (ICSMA 6)*, Proceedings of the 6th International Conference, Melbourne, Australia, August 16-20, 1982 (Pergamon Press, Oxford, 1983), pp. 983–988
11. R.Z. Valiev, R.K. Islamgaliev, I.V. Alexandrov, Prog. Mater. Sci. **45**, 103 (2000)
12. R.Z. Valiev, Y. Estrin, Z. Horita, T.G. Langdon, M.J. Zehetbauer, Y.T. Zhu, Mater. Res. Lett. **4**, 1 (2016)
13. R.Z. Valiev, A.P. Zhilyaev, T.G. Langdon, *Bulk Nanostructured Materials: Fundamentals and Applications* (Wiley, New Jersey, 2014)
14. I.V. Alexandrov, Met. Mater. Int. **7**, 565 (2001)
15. Y. Beygelzimer, Y. Estrin, R. Kulagin, Adv. Eng. Mater. **17**, 1853 (2015)
16. O. Bouaziz, H.S. Kim, Y. Estrin, Adv. Eng. Mater. **15**, 336 (2013)
17. S.O. Rogachev, S.A. Nikulin, A.B. Rozhnov, V.M. Khatkevich, T.A. Nechaykina, M.V. Gorshenkov, R.V. Sundeev, Metall. Mater. Trans. A **48**, 6091 (2017)
18. R. Lapovok, V.V. Popov Jr., Y. Qi, A. Kosinova, A. Berner, C. Xu, E. Rabkin, R. Kulagine, J. Ivanisenko, B. Baretzky, O.V. Prokof'eva, A.N. Sapronov, D.V. Prilepo, Y. Beygelzimer, Mater. Design **187**, 108398 (2020)
19. Z. Gronostajski, Z. Pater, L. Madej, A. Gontarz, L. Lisiecki, A. Lukaszek-Solek, J. Luksza, S. Mróz, Z. Muskalski, W. Muzykiewicz, M. Pietrzyk, R.E. Sliwa, J. Tomczak, S. Wiewiórowska, G. Winiarski, J. Zasadzinski, S. Ziólkiewicz, Arch. Civ. Mech. Eng. **19**, 898 (2019)
20. V.A. Andreev, V.S. Yusupov, M.M. Perkas, V.V. Prosvirnin, A.E. Shelest, S.D. Prokoshkin, IYu. Khmelevskaya, A.V. Korotitskii, S.A. Bondareva, R.D. Karelin, Russ. Metall. **2017**, 890 (2017)
21. S.A. Nikulin, T.A. Nechaikina, A.B. Rozhnov, S.O. Rogachev, VYu. Turilina, Met. Sci. Heat Treat. **60**, 229 (2018)
22. S. Prokoshkin, I. Khmelevskaya, V. Andreev, R. Karelin, V. Komarov, A. Kazakbiev, Mater. Sci. Forum **918**, 71 (2018)
23. R. Kocich, L. Kunčická, C.F. Davis, T.C. Lowe, I. Szurman, A. Macháčková, Mater. Design **90**, 379 (2016)
24. L. Kunčická, R. Kocich, K. Dvořák, A. Macháčková, Mater. Sci. Eng. A **742**, 743 (2019)
25. E.V. Avtokratova, S.V. Krymskiy, M.V. Markushev, O.S. Sitdikov, Lett. Mater. **1**, 92 (2011)
26. G. Angella, P. Bassani, A. Tuissi, D. Ripamonti, M. Vedani, Mater. Sci. Forum **503-504**, 493 (2006)
27. M.H. Shaeri, M. Shaeri, M. Ebrahimi, M.T. Salehi, S.H. Seyyedein, Prog. Nat. Sci. Mater. Int. **26**, 182 (2016)
28. S.O. Rogachev, V.A. Andreev, V.S. Yusupov, V.M. Hatkevich, E.V. Nikolaev, M.M. Perkas, S.A. Bondareva, Met. Sci. Heat Treat. **62**, 748 (2021)
29. A.M. Glezer, R.V. Sundeev, Mater. Lett. **139**, 455 (2015)
30. A.M. Glezer, L.S. Metlov, Phys. Solid State **52**, 1162 (2010)
31. E.D. Khafizova, I.P. Iskandarova, P.K. Islamgaliev, D.L. Pankratov, Lett. Mater. **5**, 399 (2015)
32. H.J. Roven, M. Liu, J.C. Werenskiold, Mater. Sci. Eng. A **483–484**, 54 (2008)
33. B. Straumal, A. Korneva, P. Zięęba, Arch. Civ. Mech. Eng. **14**, 242 (2014)
34. B.B. Straumal, V. Pontikis, A.R. Kilmametov, A.A. Mazilkin, S.V. Dobatkin, B. Baretzky, Acta Mater. **122**, 60 (2017)
35. E. Khafizova, R. Islamgaliev, G. Klevtsov, E. Merson, Mater. Phys. Mech. **24**, 232 (2015)
36. A.A. Mazilkin, B.B. Straumal, A.R. Kilmametov, T. Boll, B. Baretzky, O.A. Kogtenkova, A. Korneva, P. Zięba, Scripta Mater. **173**, 46 (2019)